crystals

MDPI

Article

Variation in Properties of Pre-Nucleation Calcium Carbonate Clusters Induced by Aggregation: A Molecular Dynamics Study

Bing-Bing Wang *, Yi Xiao and Zhi-Ming Xu

School of Energy and Power Engineering, Northeast Electric Power University, Jilin 132012, China; xiaoyi31225@163.com (Y.X.); xuzm@neepu.edu.cn (Z.-M.X.)
* Correspondence: wangbb@neepu.edu.cn

Abstract: Numerous studies have speculated calcium carbonate ($CaCO_3$) nucleation induced by pre-nucleation clusters (PNCs) aggregation. However, it is challenging for experiments to directly obtain the relationship between PNCs aggregation and nucleation. Herein, we employ molecular dynamics simulations to explore the variation during PNCs aggregation, which can describe the beginning stage of $CaCO_3$ nucleation induced by PNCs aggregation in supersaturated solutions. The results reveal that the formation of $CaCO_3$ nucleus consists of PNCs spontaneous growth, PNCs solubility equilibrium, and aggregation of PNCs inducing nucleation. The PNCs aggregation, accompanied by the variation in the configuration and stability of $CaCO_3$ aggregate, breaks the solubility equilibrium of PNCs and creates conditions for the formation of the more stable nucleus. Besides, the $CaCO_3$ nucleus with the higher coordination number and the lower hydration number form when decreasing the $CaCO_3$ concentration or increasing the temperature. This work not only sheds light on the formation of the $CaCO_3$ nucleus but also contributes to the explanation for $CaCO_3$ polymorphism.

Keywords: calcium carbonate; pre-nucleation clusters; aggregation; nucleation; molecular dynamics simulations

check for updates

Citation: Wang, B.-B.; Xiao, Y.; Xu, Z.-M. Variation in Properties of Pre-Nucleation Calcium Carbonate Clusters Induced by Aggregation: A Molecular Dynamics Study. *Crystals* **2021**, *11*, 102. https://doi.org/10.3390/cryst11020102

Received: 25 December 2020
Accepted: 22 January 2021
Published: 25 January 2021

Publisher's Note: MDPI stays neutral with regard to jurisdictional claims in published maps and institutional affiliations.

Copyright: © 2021 by the authors. Licensee MDPI, Basel, Switzerland. This article is an open access article distributed under the terms and conditions of the Creative Commons Attribution (CC BY) license (https://creativecommons.org/licenses/by/4.0/).

1. Introduction

Calcium carbonate ($CaCO_3$) is ubiquitous in marine sediments and biominerals [1,2]. Moreover, it is a common scale component from hard water resulting in practical issues [3]. Three anhydrous crystalline polymorphs of $CaCO_3$ exist in nature: calcite, aragonite, and vaterite. It has been reported that aragonite and vaterite can transform into calcite [4,5]. More interestingly, aragonite and vaterite have various morphologies, including needle-like, sheaf-of-wheat, hexagonal and dendritic crystals [6,7], highly similar to snow crystals [8]. $CaCO_3$ polymorphs with various material properties are fabricated to be used in specific industrial applications, therefore, $CaCO_3$ polymorphisms have aroused the broad concern for predicting, designing, and controlling $CaCO_3$ synthesis [7,9]. Recently, a precipitation diagram was constructed to exhibit $CaCO_3$ polymorphs depending on the supersaturation and temperature of aqueous solutions [10].

The crystallization process involves nucleation and it is widely known that nucleation plays a pivotal role in the formation of crystals [11–20]. Many efforts are increasingly devoted to the study of $CaCO_3$ nucleation to further understand its crystal formation. Classical nucleation theory (CNT) and non-classical nucleation pathways have been proposed to illustrate the nucleation events. CNT predicts that the formation of the nucleus is a consequence of monomer association in supersaturated solutions with stochastic density fluctuations [21–23]. Non-classical nucleation describes that nucleation takes place through pre-nucleation cluster (PNCs) aggregation [11,14,16,19]. The existence of PNCs in solutions as solute precursors has been proved by experiments [11,13], and the structure, dynamics, and energetics of hydrated $CaCO_3$ nano-clusters have been probed using molecular dynamics (MD) simulations [24–26].

PNCs with a hydrodynamic diameter of ~2 nm were widely detected by analytical ultracentrifugation (AUC) in the supersaturated stage near $CaCO_3$ nucleation, while larger species with hydrodynamic diameter of ~4 nm were detected in the early postnucleation stage [11]. This mutation in cluster size during nucleation supports the hypothesis of non-classical nucleation. Subsequent experiments confirmed that diameters of PNCs are in the range of 0.6–4 nm [13]. However, it is not clear whether PNCs aggregation triggers nucleation. Nowadays, MD simulations were performed to probe microscopic evidence for non-classical nucleation. The Ca-C coordination number of PNCs, a precursor of nucleation, generated in supersaturated $CaCO_3$ solutions at ambient temperature is close to two, which is similar to the chain-like model [25]. While biogenic species of ACC, an intermediate product of the crystallization, have coordination numbers commensurate with crystalline species [17]. These PNCs are stable and remain in solubility equilibrium in the pre-nucleation stage instead of dissolving spontaneously. The PNCs were referred to as dynamically ordered liquid-like oxyanion polymer (DOLLOP) due to the remarkable flexibility. Through artificially adding ion pairs to a fixed $CaCO_3$ cluster, the Ca-C coordination number increased from two to three during the cluster growth, and the free energy monotonically decreased [26]. It is noted that the Ca-C coordination number in $CaCO_3$ clusters is slightly larger than that formed by spontaneous reaction in supersaturated solutions [25]. In the simulation [26], the initial PNC was a hydrated $CaCO_3$ cluster with 22 formula units built by adding ion pairs to a fixed cluster, and the amorphous calcium carbonate (ACC) structure was constructed by PNCs aggregation. In view of the lower concentration and temperature in the previous work [25], PNCs have a lower diffusion coefficient so it is difficult to observe the phenomenon of aggregation for different PNCs in a limited simulation time. However, there is little insight into the variation of PNCs properties during the aggregation, which is significant for understanding $CaCO_3$ nucleation and polymorphism. Furthermore, the aragonite is generated at low concentrations and high temperatures, while the vaterite is generated at high concentrations and ambient temperatures [10]. How these conditions affect the $CaCO_3$ crystal is not fully understood.

We present the results of an MD study of the spontaneous growth and aggregation of PNCs in supersaturated $CaCO_3$ solutions to explore the beginning stage of $CaCO_3$ nucleation. The coordination number, hydration number, potential energy, and diffusion coefficient are calculated to analyze the variation of PNCs properties. This work provides evidence for the beginning stage of $CaCO_3$ nucleation induced by PNCs aggregation. Moreover, the influences of $CaCO_3$ concentration and temperature on PNCs aggregation are discussed to gain a better understanding of $CaCO_3$ polymorphism.

2. Simulation Section

In the simulations, two models were used to simulate the spontaneous growth and aggregation of PNCs in the supersaturated solution. Model I: cubic boxes were built with 5800 water molecules. To analyze the influence of $CaCO_3$ concentration, the cubic boxes were separately added 50, 75, 100, 125, and 150 Ca^{2+} and CO_3^{2-}, and the corresponding concentration was 0.48, 0.72, 0.96, 1.2, and 1.44 mol/L, respectively. Model II: cubic boxes where the number of Ca^{2+} and CO_3^{2-} was fixed at 50, consisted of 2900, 3850, and 5800 water molecules, respectively, and the corresponding concentration was 0.48, 0.72, and 0.96 mol/L. This model was only used to explore the pre-nucleation process, and the higher concentrations of 1.2 and 1.44 mol/L were not simulated.

Model I was adopted to mainly discuss the variation of properties of PNCs, and model II was built to verify the result's reasonability. At a higher temperature, it can take less time for PNCs to aggregate [24], which may be related to the self-diffusion coefficient of PNCs affected by temperature. Therefore, in order to observe the phenomenon of PNCs aggregation in the limited simulation time, the temperature was set to 360 K. Recently, experimental observation of $CaCO_3$ crystallization suggests that vaterite and calcite are generally formed at ambient temperature, while aragonite becomes the main phase above

75 °C [10]. Therefore, the simulations with model I at temperatures of 300, 330, and 360 K were performed to reveal the effect of temperature on $CaCO_3$ pre-nucleation.

All simulations were performed with the program LAMMPS [27]. The intermolecular parameters of Raiteri et al. were used [28], and the SPC/Fw water model was adopted [29]. The intramolecular parameters from Demichelis et al. were employed which accurately describe the vibrational spectrum of carbonate [25]. The simulation system was stabilized for 0.2 ns in the NPT ensemble with a chain of five Nosé-Hoover thermostats, the thermostat and barostat relaxation times were 0.1 and 1 ps, respectively. Then, the simulation was performed in the NVT ensemble with Nosé-Hoover thermostats to simulate the growth and aggregation of PNCs—the thermostat relaxation time was 0.1 ps. Particle motion was solved by the Velocity-Verlet algorithm with a time step of 1 fs [30]. The long-range electrostatic interaction was calculated using the PPPM algorithm with an accuracy of 10^{-4} [31].

Figure 1a–d present the evolution of radial distribution functions (RDFs) for Ca-Ca, Ca-C, Ca-O (O refer to oxygen in carbonate), and Ca-O_w (O_w refer to oxygen in water), respectively. To distinguish free ions and ion pairs, calcium is within in PNCs or aggregate when its coordination numbers of Ca-Ca and Ca-C are larger than zero. The coordination number of Ca^{2+} in PNCs or aggregate is the average value, calculated by the total coordination number of Ca^{2+} divided by the amount of Ca^{2+}. The cutoff for coordination numbers of Ca-Ca and Ca-C was 7.1 and 3.9 Å, respectively (refer to the second valley of radial RDFs as shown in Figure 1a,b). Besides, Ca-O and Ca-O_w coordination numbers in PNCs or aggregate were also counted where the cutoffs were set to 3.1 Å as displayed in Figure 1c,d.

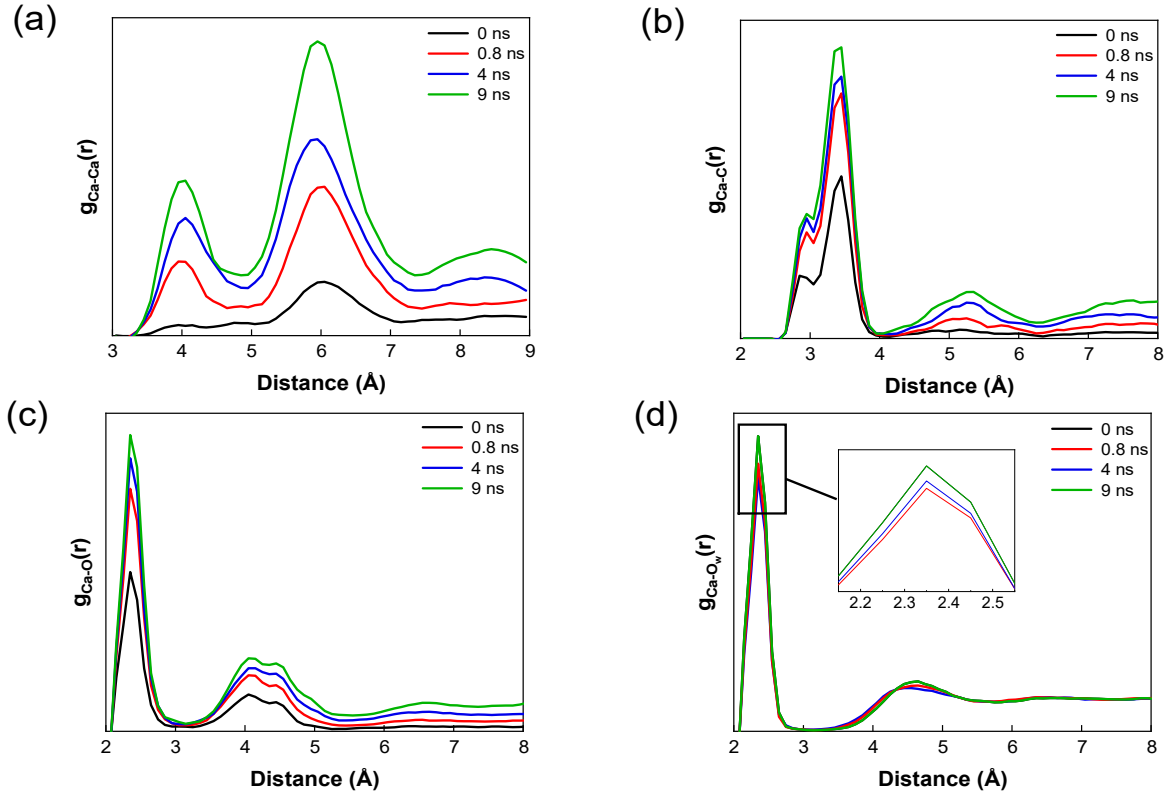


Figure 1. Radial distribution functions (RDFs) for (**a**) Ca-Ca, (**b**) Ca-C, (**c**) Ca-O, and (**d**) Ca-O_w in 0.96 mol/L $CaCO_3$ solution at 360 K. Here, O and O_w refer to oxygens in the carbonate and water, respectively.

The Ca-O_w coordination number represents the hydration number. There is no obvious peak near 4 Å at 0 ns, while the peak near 6 Å is observed as presented in Figure 1a suggesting that two calcium ions coordinated with each other are mainly paired with

different oxygens of a carbonate [32]. Peaks in RDFs of Ca-Ca, Ca-C, and Ca-O increase during PNCs growth and aggregation, while they slightly decrease for Ca-O_w as shown in Figure 1a–d. These variations display the trend for the combining of Ca^{2+} and CO_3^{2-}.

The potential energy of Ca^{2+} in clusters was monitored to study the thermodynamics properties of PNCs or aggregates versus the reaction time. The equilibrium state can be estimated by the variation of internal energy, which is the sum of potential energy and kinetic energy. For a certain temperature, the variation of the potential energy for Ca^{2+} in clusters is much higher than its kinetic energy (more than one order of magnitude). Therefore, the variation of potential energy is discussed in the work.

According to the Stokes-Einstein relation, the self-diffusion coefficient (D) is obtained by Equation (1) [33].

$$D = \frac{1}{6}\frac{\left\langle (\delta r)^2 \right\rangle}{\Delta t}, \quad (1)$$

where is the mean square displacement (MSD) within the time interval (Δt).

The pre-nucleation instant is defined as the moment located near the extremum of the coordination number and potential energy when the aggregate size reaches the maximum for the first time in stage III. The average value of each parameter in the range of 0.2 ns near the pre-nucleation time is taken as the parameter of the nucleus.

3. Results and Discussion

3.1. Evolution of Nucleation

Snapshots of PNCs growth and aggregation in the supersaturated solution with a $CaCO_3$ concentration of 0.96 mol/L at 360 K are shown in Figure 2a. Firstly, ion pairs or chain-like PNCs (Figure S1) are formed through the binding between Ca^{2+} and CO_3^{2-} and subsequently, they grow to larger chain-like PNCs by collisions with ions, ion pairs, and/or PNCs chains. Due to the consumption of free ions and ion pairs in the solution, PNCs reach solubility equilibrium. It is worth noting that three PNCs are near each other at t = 4.6 ns and then the aggregation of PNCs occurs. A larger aggregate forms and its diameter is approximately 4.5 nm, close to the hydrodynamic diameter of clusters (4 nm) in the early postnucleation stage detected utilizing AUC [11,13].

The evolution of the simulation process can be divided into four stages: PNCs spontaneous growth, PNCs solubility equilibrium, aggregation of PNCs inducing nucleation, and the postnucleation stage. In the PNCs spontaneous growth stage, short chains grow to larger PNCs, and the number of ions in the PNCs increases (Figure 2b). The proportion for CN (coordination number) = 1 of Ca-C pairs decreased from 0.44 to 0.12 at t = 2.8 ns (Figure 2c), while the portion for CN = 2 increased to 0.64 implying that the chain-like PNCs dominantly exist in the aqueous solution and they had not yet evolved into ACC with the higher coordination number. In addition, the average Ca-C coordination number in PNCs increased from 1.57 to 2.2. Correspondingly, the hydration number decreased from 5.75 to 5.23 (Figure 2d). As a result, the stable PNCs with the lower potential energy (Figure 2e) were obtained, which suggests that the growth of PNCs was spontaneous [26]. It is noted that the number of ions in PNCs remarkably fluctuated at 2.8 ns (Figure 2b) because of the transient contact and the separation of PNCs. Subsequently in the PNCs solubility equilibrium, due to the reduction of free ions or ion pairs in the PNCs growth stage, PNCs growth terminated and they were stable in the solution. Therefore, the number of ions in PNCs, coordination number, hydration number, and potential energy (Figure 2b,d,e) were almost constant, illustrating that the structures and thermodynamic properties of PNCs maintained unchanged.

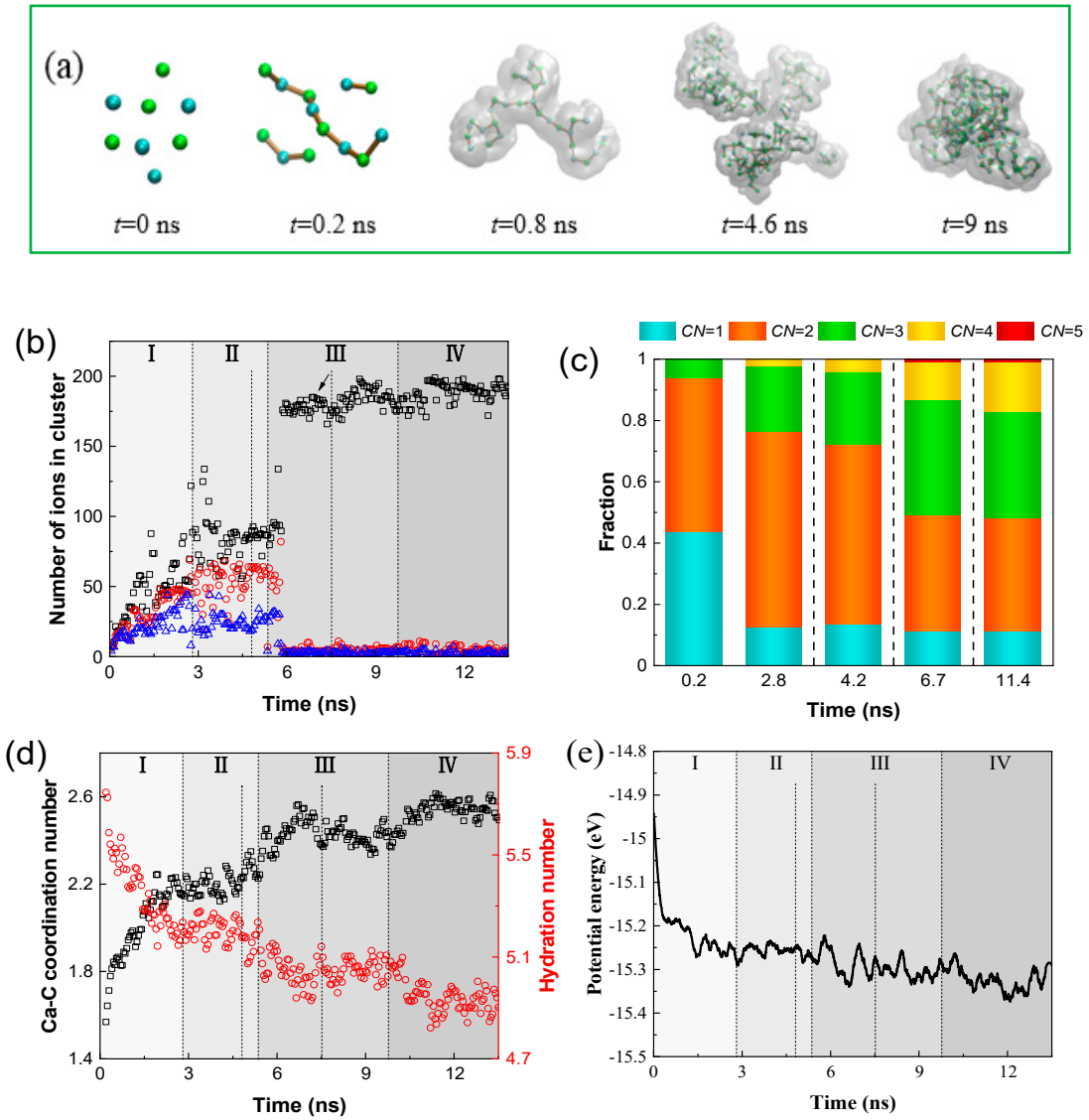


Figure 2. (**a**) MD simulations snapshots for PNCs growth and aggregation in the aqueous solution with 0.96 mol/L $CaCO_3$ at 360 K. The green, cyan, and gray colors represent Ca^{2+}, CO_3^{2-}, and hydration shell, respectively. The final cluster by PNCs aggregation is referred to as "aggregate". (**b**) Evolution of the number of ions in the three largest clusters. The black, red, and blue represent the first, second, and third large-size clusters, respectively. The nucleation instant is marked with an arrow. (**c**) Fraction of coordination number CN = 1–5 of Ca-C pairs at various instants. (**d**) Evolution of Ca-C coordination number and hydration number for Ca ions in the PNCs or aggregate. (**e**) Evolution of potential energy of calcium ions in the PNCs or aggregate.

Driven by Brownian motion, PNCs aggregation occurs in the vicinity of 5.7 ns (Figure 2b), which breaks the solubility equilibrium of PNCs. The number of ions in the largest PNCs nd the Ca-C coordination number instantly increase, while the hydration number and potential energy reduce (Figure 2d,e, the third stage). The Ca-C coordination number of the aggregate has exceeded two, which shows that the aggregate is gradually distinguished from chain-like PNCs and evolves into ACC. Meanwhile, the variation of the Ca-C coordination number is coupled with dehydration (Figure 2d). These variations suggest that a more stable structure forms after rearrangement of the aggregate. In order to clarify the relationship between PNCs aggregation and the beginning stage of $CaCO_3$ nucleation, we analyze the reaction process based on chemical equilibrium as follows.

According to the discussion in Section S2 of the Supplementary Materials, the reaction process before PNCs aggregation consists of the formation of ion pairs and the growth of PNCs, and the corresponding equilibrium constant (K) can be written as:

$$Ca^{2+} + CO_3^{2-} \rightleftharpoons [CaCO_3]^0_{pair} \quad K_{pair} = \frac{a_{pair}\left(Ca^{2+}\right)}{a_{free}\left(Ca^{2+}\right)a_{free}\left(CO_3^{2-}\right)} \tag{2}$$

$$[CaCO_3]^0_{pair} \rightleftharpoons [CaCO_3]^0_{PNCs} \quad K_{PNCs} = \frac{a_{PNCs}\left(Ca^{2+}\right)}{a_{pair}\left(Ca^{2+}\right)} \tag{3}$$

Since K_{PNCs} is constant under the specific condition (Supplementary Materials Section S2), the activity and properties of PNCs maintain invariant in the solubility equilibrium stage. However, the potential energy of calcium in PNCs will decrease after aggregation (Figure 2e) due to the structural rearrangement of aggregate (Figure 2d). Consequently, a more stable cluster, which is generally called the nucleus, is formed and breaks the solubility equilibrium.

$$[CaCO_3]^0_{PNCs} \rightarrow [CaCO_3]_{nucleus} \tag{4}$$

With respect to Equation (4), the formation of the nucleus with the lower potential energy relies on the consumption of PNCs, and it breaks the solubility equilibrium of PNCs (Equations (2) and (3)). Hence, the activity of free ions will decrease with the formation of the stable nucleus after aggregation. The decreasing of free ions activity in solution caused by aggregation can be related to the $CaCO_3$ pre-nucleation. Meanwhile, the activity of free ions will decrease below the solubility of PNCs without aggregation. Therefore, the smaller PNCs clusters will be generated by the PNCs dissociation. Subsequently, liquid-like nuclei and smaller clusters further aggregate until the generation of more stable solid-state ACC. The total equilibrium equation after nucleation is written as:

$$Ca^{2+} + CO_3^{2-} \rightleftharpoons [CaCO_3]_{ACC} \quad K_{ACC} = \frac{1}{a_{free}\left(Ca^{2+}\right)a_{free}\left(CO_3^{2-}\right)}, \tag{5}$$

where the activity of the solid-state ACC will not appear in the expression of K_{ACC}. The activity of free ions will be constant after the generation of solid-state ACC based on Equation (5).

For the postnucleation stage, there is no addition of ions in the simulation, thus aggregate does not grow. The aggregate belongs to a dense liquid phase since the diffusion coefficient is approximately equal to 3.5×10^{-8} m^2/s (Figure 3a, the third stage), which is between diffusion coefficients of water and ACC [26,34,35]. Therefore, properties of the aggregate fluctuate with its dissociation and re-aggregation dominated by solubility equilibrium in the postnucleation stage (Figure 2b,d,e). Due to the limited calculations, this work mainly focuses on the variation of PNCs induced by aggregation during the beginning stage of $CaCO_3$ nucleation, the simulation ends at the forming of $CaCO_3$ nucleus.

As presented in Figure 3a, at the beginning of the reaction, the diffusion coefficient of Ca^{2+} drops sharply due to the binding of free ions. Meanwhile, the diffusion coefficient also reduces for water molecules bound around the ions due to hydration (Figure 3b). Then the diffusion coefficient of ions and water molecules respectively remain at the lower values when the larger $CaCO_3$ clusters have formed, and the diffusion coefficient of Ca^{2+} decreases slightly due to the subtle changes in aggregate properties. It can be concluded that the formation of the $CaCO_3$ nucleus consists of PNCs spontaneous growth, PNCs solubility equilibrium, and aggregation of PNCs inducing pre-nucleation.

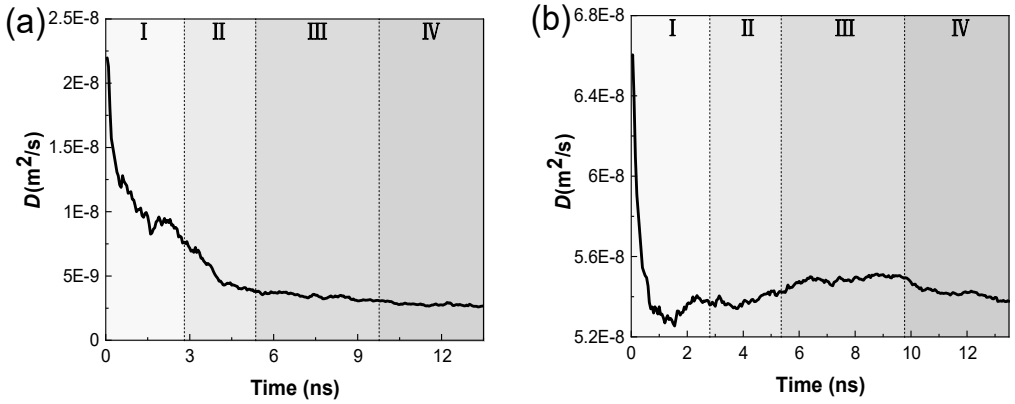


Figure 3. Diffusion coefficient of (**a**) Ca^{2+} and (**b**) water molecules. Since clusters belong to the dense liquid phase, the diffusion coefficient of Ca^{2+} is lower than that of water molecules.

3.2. Effect of Concentration

The growth and aggregation of PNCs for 0.48, 0.72, 1.2, and 1.44 mol/L $CaCO_3$ solutions are also simulated to reveal the influence of concentration (Figures S2–S5). For the concentrations of 0.48 and 0.72 mol/L, the evolution of PNCs is similar to that of 0.96 Tmol/L. While for higher concentrations of 1.2 and 1.44 mol/L, it is worth noting that the evolution of $CaCO_3$ clusters is highly similar to the phase separation via a spinodal decomposition (Figure 4) [16]. At the beginning of the reaction, ions are basically evenly distributed in the solution (Figure 4, t = 1.31 ns). Then, the characteristic channel-like bicontinuous pattern forms (Figure 4, t = 3.15–10.96 ns), while PNCs and nuclei in the nucleation are surrounded by the solvent at low $CaCO_3$ concentrations (Figure 2a) [16]. The thermodynamic and kinetic properties of these structures also change continuously (Figures S4 and S5 in Supplementary Materials), which is in agreement with the notion that no energy barrier needs to be overcome for the spinodal decomposition [16,36]. Consistent with the nucleation, the spinodal decomposition is achieved via continuous dissociation and re-aggregation of the nanoscopic liquid phase in the phase separation.

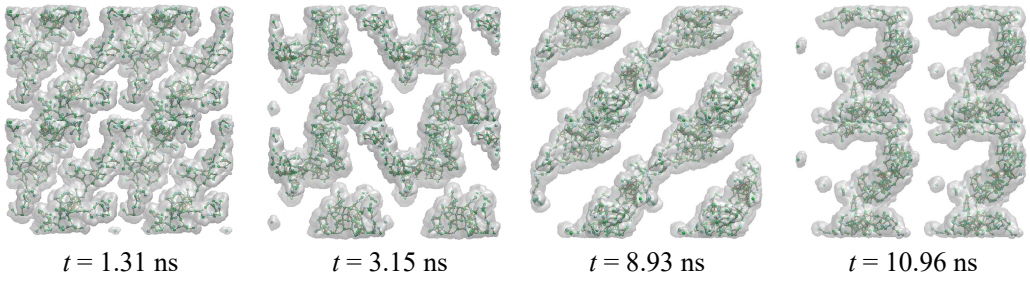


Figure 4. D simulations snapshots in the aqueous solution with $CaCO_3$ concentration of 1.44 mol/L at 360 K. In order to observe the phenomenon of phase separation clearly, the snapshots were extended a periodic boundary in the x and y directions, respectively. The green, cyan, and gray colors represent Ca^{2+}, CO_3^{2-}, and the hydration shell, respectively.

For the lower $CaCO_3$ concentration of 0.48 and 0.72 mol/L, PNCs with the smaller size have a high diffusion coefficient, which results in the shorter stage II (Figures S2 and S3). In contrast, the number density may be dominant for the extremely lower $CaCO_3$ concentration so that it takes a longer time for PNCs aggregation [11,19]. Therefore, the nucleation time is dependent on both the number density and the diffusion coefficient of PNCs. However, it is impossible to obtain the law of nucleation induction time versus concentration in a statistically meaningful way due to the limited simulations.

The coordination number and the hydration number of the aggregate are compared for various $CaCO_3$ concentrations (Figure 5). When $CaCO_3$ concentration ranges from

0.48 to 0.96 mol/L, the Ca-C coordination number in aggregate decreases from 2.62 to 2.53, and the hydration number increases from 4.86 to 5.01. While increasing $CaCO_3$ concentrations to 1.2 and 1.44 mol/L, the Ca-C coordination number increases and the hydration number reduces. Furthermore, a new model is built where the number of ions is constant and the water number changes (Figures S6 and S7). The effect of $CaCO_3$ concentration on Ca-C coordination number and hydration number (Figure S8) is consistent with the above description, verifying the rationality of the simulation results. Recently, it has been reported that the solubility of ACC generated in the aqueous solution varies with $CaCO_3$ supersaturation [19], and the aragonite with larger coordination number is formed under the lower $CaCO_3$ concentration [10]. The reason for these phenomena can be speculated to the effect of $CaCO_3$ concentration on the properties of aggregate after PNCs aggregation.

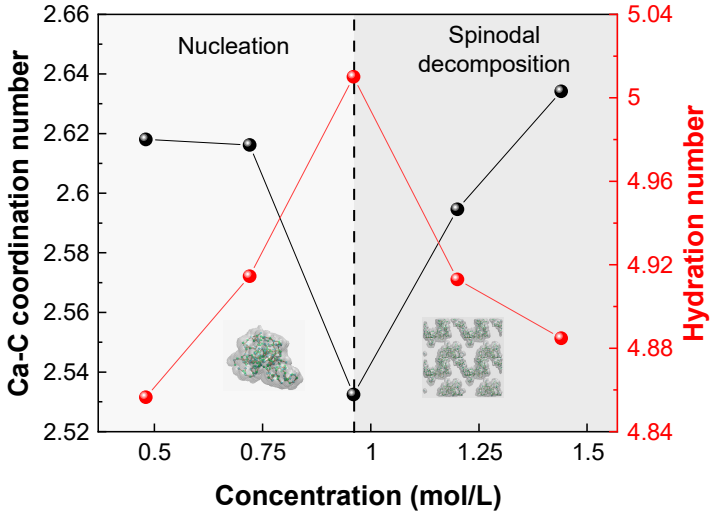


Figure 5. Ca-C coordination number and hydration number of aggregates for various $CaCO_3$ concentrations at 360 K. There are two phase-separation pathways: nucleation and spinodal decomposition. The evolution of PNCs at 0.96 mol/L belongs to the nucleation zone. The dotted line is defined as the boundary for two pathways.

3.3. Effect of Temperature

The influence of temperature (300, 330, and 360 K) on the nucleation for 0.72 mol/L $CaCO_3$ supersaturation is shown in Figure 6 (the evolution of nucleation at each temperature was respectively shown in Figures S3, S9, and S10). When the temperature increases from 300 to 360 K, the Ca-C coordination number increases from 2.18 to 2.62 and the hydration number reduces from 5.38 to 4.92 (Figure 6a). These variations imply the greater impact of temperature on the aggregate structure compared with the influence of $CaCO_3$ concentrations (Figure 5). Ca-O coordination number in PNCs at 300 K in the second stage is approximately two (Figure S11a), which equals to that of proto-vaterite ACC and proto-calcite ACC [37]. Meanwhile, the Ca-O coordination number is slightly larger at 330 K (Figure S11b) which is similar to the proto-aragonite ACC generated at a higher temperature [38]. The above conclusion is identical with that of the nucleation product having a higher Ca-O coordination number at high temperature as obtained by previous experiments. The variation of the coordination number versus temperature may be the result of the combined effect of temperature on the potential energy and the diffusion.

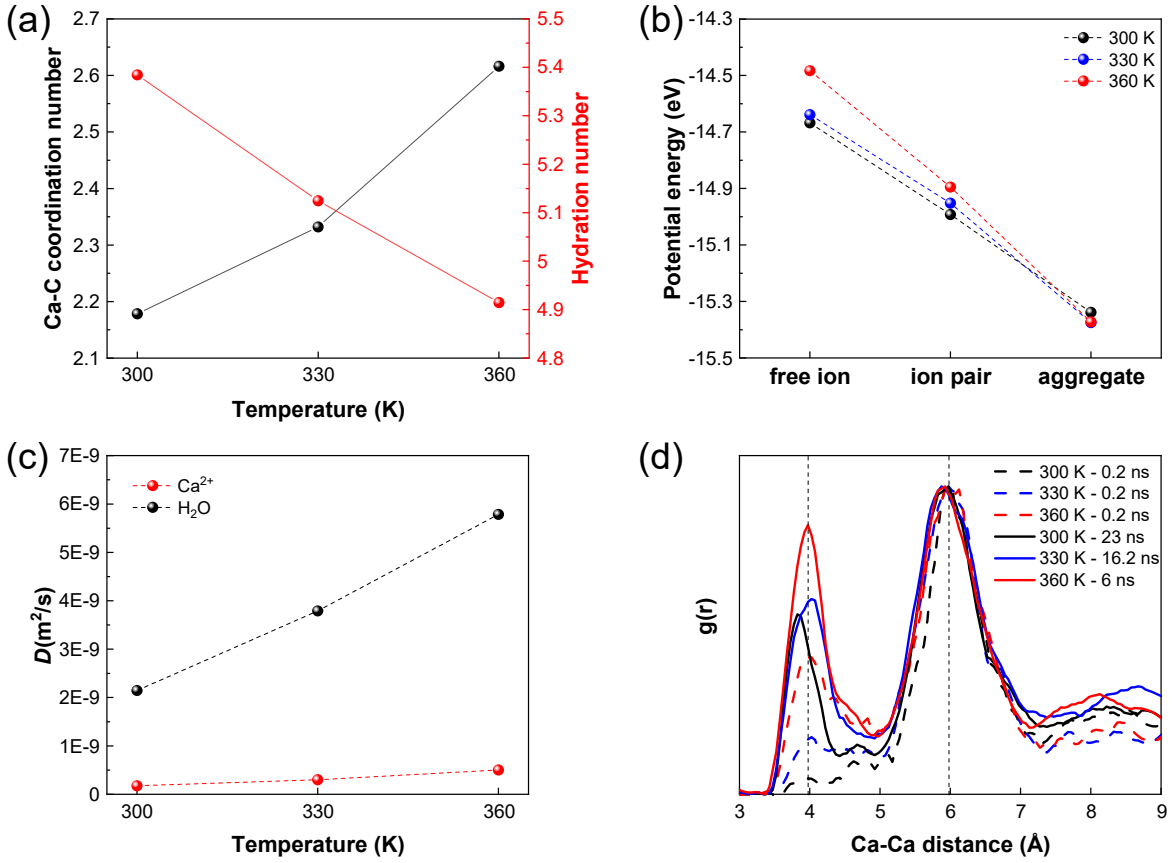


Figure 6. Influence of temperature (300, 330, and 360 K) on nucleation for 0.72 mol/L supersaturated $CaCO_3$ solution. (**a**) Ca-C coordination number and hydration number of aggregate. (**b**) Potential energy of Ca^{2+} with different forms. (**c**) Diffusion coefficient for water and Ca^{2+}. (**d**) Radial distribution function of Ca-Ca distance ($g_{Ca\text{-}Ca}$) before and after nucleation. Note that the absolute magnitude of $g_{Ca\text{-}Ca}$ has been scaled through normalization

Free ions and ion pairs have higher potential energy and the aggregate has lower potential energy at the same temperature (Figure 6b). The potential energy of ions and ion pairs increases at the higher temperature, indicating that ions and ion pairs are much easier to associate [39]. In comparison, the potential energy of aggregate slightly reduces, suggesting its more stable structure at the higher temperature. Water molecules have a larger diffusion coefficient in aqueous solutions than Ca^{2+} in PNCs, in addition, the diffusion coefficient of water and Ca^{2+} in PNCs increases with the temperature, which indicates that a high temperature promotes the movement of ions (Figure 6c).

The previous studies focusing on ACC structure observed that the radial distribution function of Ca-Ca distance has two significant peaks at ~4 and 6 Å, and the value at the first peak is higher than the second peak for ACC [28,39–41]. In our simulation, two peaks at ~4 and 6 Å are also observed in the Ca-Ca RDFs before and after $CaCO_3$ nucleation (Figure 6d), and the peak has higher values at a raised temperature implying a better range order within the $CaCO_3$ aggregate [32]. The first peak is lower than the second peak, which differs from the results for ACC [28,39–41]. However, it can be found that the first peak increases with PNCs evolution (Figure 6d), which displays a transformation tendency of structures from PNCs into ACC.

4. Conclusions

In summary, the beginning stage of the $CaCO_3$ nucleation process can be divided into three stages: PNCs spontaneous growth, PNCs solubility equilibrium, and aggregation of PNCs inducing nucleation. In the first stage, chain-like PNCs with a coordination

number equal to two can be formed. These PNCs are stable and will not spontaneously dehydrate through twisting or folding. However, PNCs aggregation leads to variation in PNCs properties including an increase in Ca-C coordination number, as well as reductions in dehydration, potential energy, and diffusion coefficient. The behavior similar to phase separation via spinodal decomposition is observed for the higher $CaCO_3$ concentration of 1.2 and 1.44 mol/L. The variation in these properties is attributed to the rearrangement of PNCs during aggregation in the mass transfer process, which can be commendably used to explain the nucleation behavior in titration experiments [11].

PNCs aggregation induces the formation of the stable $CaCO_3$ nucleus and breaks the solubility equilibrium. Meanwhile, the $CaCO_3$ nucleus grows through the diffusion and collision of ions, ion pairs, or clusters. Then, the concentration of ions decreases below the solubility of PNCs without aggregation. Therefore, the smaller clusters are generated by the dissociation of these PNCs. Subsequently, the liquid-like nucleus and smaller clusters further aggregate until generation of the solid-state ACC. The number of clusters with several nanometer diameters decreases rapidly after nucleation observed using small-angle X-ray scattering, while clusters with several tens of nanometers grow unceasingly but their number maintains constant [42]. In addition, the influence of the concentration and temperature on the nucleation and crystallization may attribute to their effect on the growth and aggregation of PNCs, which controls the properties of the nucleus. The nucleus with a higher coordination number forms when decreasing the $CaCO_3$ concentration or increasing the temperature, indicating that at a higher temperature or lower concentration of the aqueous solution, it is easier to fabricate the $CaCO_3$ polymorph with the high coordination number, such as aragonite.

Supplementary Materials: The following are available online at https://www.mdpi.com/2073-4352/11/2/102/s1, Figure S1: Snapshots for PNCs spontaneous growth in the aqueous solution with $CaCO_3$ concentration of 0.96 mol/L at 360 K., Figure S2: Evolution of properties of PNCs or aggregate in the aqueous solution with $CaCO_3$ concentration of 0.48 mol/L at 360 K., Figure S3: Evolution of properties of PNCs or aggregate in the aqueous solution with $CaCO_3$ concentration of 0.72 mol/L at 360 K., Figure S4: Evolution of spinodal decomposition in the aqueous solution with $CaCO_3$ concentration of 1.2 mol/L at 360 K., Figure S5: Evolution of spinodal decomposition in the aqueous solution with $CaCO_3$ concentration of 1.44 mol/L at 360 K., Figure S6: Evolution of nucleation in the aqueous solution with $CaCO_3$ concentration of 0.96 mol/L at 360 K in model II., Figure S7: Evolution of nucleation in the aqueous solution with $CaCO_3$ concentration of 0.72 mol/L at 360 K in model II., Figure S8: Ca-C coordination number and hydration number of aggregate for various $CaCO_3$ concentrations at 360 K in model II., Figure S9: Evolution of nucleation in the aqueous solution with $CaCO_3$ concentration of 0.72 mol/L at 300 K., Figure S10: Evolution of nucleation in the aqueous solution with $CaCO_3$ concentration of 0.72 mol/L at 330 K., Figure S11: Evolution of Ca-O coordination number and hydration number for Ca^{2+} in the PNCs or aggregate for 0.72 mol/L $CaCO_3$ solution at the temperature of 300 K and 330 K.

Author Contributions: Conceptualization, B.-B.W. and Y.X.; methodology, Y.X.; software, Y.X.; validation, B.-B.W., Y.X., and Z.-M.X.; investigation, Y.X.; resources, B.-B.W.; data curation, Y.X.; writing—original draft preparation, B.-B.W. and Y.X.; writing—review and editing, B.-B.W. and Z.-M.X.; supervision, B.-B.W. and Z.-M.X.; funding acquisition, B.-B.W. and Z.-M.X. All authors have read and agreed to the published version of the manuscript.

Funding: This research was funded by National Natural Science Foundation of China grant numbers 51706038 and 51976028.

Institutional Review Board Statement: Not applicable.

Informed Consent Statement: Not applicable.

Data Availability Statement: Data is contained within the article. The data presented in this study can be seen in the content above.

Conflicts of Interest: The authors declare no conflict of interest.

References

1. Morse, J.W.; Arvidson, R.S.; Lüttge, A. Calcium Carbonate Formation and Dissolution. *Chem. Rev.* **2007**, *107*, 342–381. [CrossRef] [PubMed]
2. Meldrum, F.C. Calcium carbonate in biomineralisation and biomimetic chemistry. *Int. Mater. Rev.* **2003**, *48*, 187–224. [CrossRef]
3. Andritsos, N.; Karabelas, A.J. Calcium carbonate scaling in a plate heat exchanger in the presence of particles. *Int. J. Heat Mass Transf.* **2003**, *46*, 4613–4627. [CrossRef]
4. Ogino, T.; Suzuki, T.; Sawada, K. The formation and transformation mechanism of calcium carbonate in water. *Geochim. Cosmochim. Acta* **1987**, *51*, 2757–2767. [CrossRef]
5. Nielsen, M.H.; Aloni, S.; De Yoreo, J.J. In situ TEM imaging of $CaCO_3$ nucleation reveals coexistence of direct and indirect pathways. *Science* **2014**, *345*, 1158–1162. [CrossRef]
6. Kawano, J.; Shimobayashi, N.; Miyake, A.; Kitamura, M. Precipitation diagram of calcium carbonate polymorphs: Its construction and significance. *J. Phys. Condens. Matter.* **2009**, *21*, 425102. [CrossRef]
7. Xu, A.W.; Dong, W.F.; Antonietti, M.; Cölfen, H. Polymorph Switching of Calcium Carbonate Crystals by Polymer-Controlled Crystallization. *Adv. Funct. Mater.* **2008**, *18*, 1307–1313. [CrossRef]
8. Libbrecht, K.G. The physics of snow crystals. *Rep. Prog. Phys.* **2005**, *68*, 855–895. [CrossRef]
9. Nan, Z.; Chen, X.; Yang, Q.; Wang, X.; Shi, Z.; Hou, W. Structure transition from aragonite to vaterite and calcite by the assistance of SDBS. *J. Colloid Interface Sci.* **2008**, *325*, 331–336. [CrossRef]
10. Ma, M.; Wang, Y.; Cao, X.; Lu, W.; Guo, Y. Temperature and supersaturation as key parameters controlling the spontaneous precipitation of calcium carbonate with distinct physico-chemical properties from pure aqueous solutions. *Cryst. Growth Des.* **2019**, *19*, 6972–6988. [CrossRef]
11. Gebauer, D.; Völkel, A.; Cölfen, H. Stable Prenucleation Calcium Carbonate Clusters. *Science* **2008**, *322*, 1819–1822. [CrossRef]
12. Zahn, D. Thermodynamics and Kinetics of Prenucleation Clusters, Classical and Non-Classical Nucleation. *ChemPhysChem* **2015**, *16*, 2069–2075. [CrossRef] [PubMed]
13. Pouget, E.M.; Bomans, P.H.H.; Goos, J.A.C.M.; Frederik, P.M.; de With, G.; Sommerdijk, N.A.J.M. The Initial Stages of Template-Controlled $CaCO_3$ Formation Revealed by Cryo-TEM. *Science* **2009**, *323*, 1455–1458. [CrossRef] [PubMed]
14. Gebauer, D.; Cölfen, H. Prenucleation clusters and non-classical nucleation. *Nano Today* **2011**, *6*, 564–584. [CrossRef]
15. Quigley, D.; Freeman, C.L.; Harding, J.H.; Rodger, P.M. Sampling the structure of calcium carbonate nanoparticles with metadynamics. *J. Chem. Phys.* **2011**, *134*, 44703. [CrossRef]
16. Gebauer, D.; Kellermeier, M.; Gale, J.D.; Bergström, L.; Cölfen, H. Pre-nucleation clusters as solute precursors in crystallization. *Chem. Soc. Rev.* **2014**, *43*, 2348–2371. [CrossRef]
17. Kelton, K.F.; Frenkel, D. Special Topic on Nucleation: New Concepts and Discoveries. *J. Chem. Phys.* **2016**, *145*, 211501. [CrossRef]
18. Du, H.; Amstad, E. Water: How does it influence the $CaCO_3$ formation? *Angew. Chem. Int. Ed.* **2020**, *59*, 1798–1816. [CrossRef]
19. Avaro, J.T.; Wolf, S.L.P.; Hauser, K.; Gebauer, D. Stable Pre-nucleation Calcium Carbonate Clusters Define Liquid-Liquid Phase Separation. *Angew. Chem. Int. Ed.* **2020**, *59*, 6155–6159. [CrossRef]
20. Jin, B.; Liu, Z.; Tang, R. Recent experimental explorations of non-classical nucleation. *CrystEngComm* **2020**, *22*, 4057–4073. [CrossRef]
21. Smeets, P.J.M.; Cho, K.R.; Kempen, R.G.E.; Sommerdijk, N.A.J.M.; De Yoreo, J.J. Calcium carbonate nucleation driven by ion binding in a biomimetic matrix revealed by in situ electron microscopy. *Nat. Mater.* **2015**, *14*, 394–399. [CrossRef] [PubMed]
22. Smeets, P.J.M.; Finney, A.R.; Habraken, W.J.E.M.; Nudelman, F.; Friedrich, H.; Laven, J.; De Yoreo, J.J.; Rodger, P.M.; Sommerdijk, N.A.J.M. A classical view on nonclassical nucleation. *Proc. Natl. Acad. Sci. USA* **2017**, *114*, E7882–E7890. [CrossRef] [PubMed]
23. Henzler, K.; Fetisov, E.O.; Galib, M.; Baer, M.D.; Legg, B.A.; Borca, C.; Xto, J.M.; Pin, S.; Fulton, J.L.; Schenter, G.K.; et al. Supersaturated calcium carbonate solutions are classical. *Sci. Adv.* **2018**, *4*, eaao6283. [CrossRef] [PubMed]
24. Tribello, G.A.; Bruneval, F.; Liew, C.; Parrinello, M. A Molecular Dynamics Study of the Early Stages of Calcium Carbonate Growth. *J. Phys. Chem. B* **2009**, *113*, 11680–11687. [CrossRef]
25. Demichelis, R.; Raiteri, P.; Gale, J.D.; Quigley, D.; Gebauer, D. Stable prenucleation mineral clusters are liquid-like ionic polymers. *Nat. Commun.* **2011**, *2*, 590. [CrossRef] [PubMed]
26. Wallace, A.F.; Hedges, L.O.; Fernandez-Martinez, A.; Raiteri, P.; Gale, J.D.; Waychunas, G.A.; Whitelam, S.; Banfield, J.F.; De Yoreo, J.J. Microscopic Evidence for Liquid-Liquid Separation in Supersaturated $CaCO_3$ Solutions. *Science* **2013**, *341*, 885–889. [CrossRef] [PubMed]
27. Plimpton, S. Fast Parallel Algorithms for Short-Range Molecular Dynamics. *J. Comp. Phys.* **1995**, *117*, 1–19. [CrossRef]
28. Raiteri, P.; Gale, J.D. Water Is the Key to Nonclassical Nucleation of Amorphous Calcium Carbonate. *J. Am. Chem. Soc.* **2010**, *132*, 17623–17634. [CrossRef]
29. Wu, Y.; Tepper, H.L.; Voth, G.A. Flexible simple point-charge water model with improved liquid-state properties. *J. Chem. Phys.* **2006**, *124*, 024503. [CrossRef]
30. Swope, W.C.; Andersen, H.C.; Berens, P.H.; Wilson, K.R. A computer simulation method for the calculation of equilibrium constants for the formation of physical clusters of molecules: Application to small water clusters. *J. Chem. Phys.* **1982**, *76*, 637–649. [CrossRef]
31. Beckers, J.V.L.; Lowe, C.P.; De Leeuw, S.W. An Iterative PPPM Method for Simulating Coulombic Systems on Distributed Memory Parallel Computers. *Mol. Simulat.* **1998**, *20*, 369–383. [CrossRef]

32. Goodwin, A.L.; Michel, F.M.; Phillips, B.L.; Keen, D.A.; Dove, M.T.; Reeder, R.J. Nanoporous Structure and Medium-Range Order in Synthetic Amorphous Calcium Carbonate. *Chem. Mater.* **2010**, *22*, 3197–3205. [CrossRef]
33. Jung, G.Y.; Shin, E.; Park, J.H.; Choi, B.-Y.; Lee, S.-W.; Kwak, S.K. Thermodynamic Control of Amorphous Precursor Phases for Calcium Carbonate via Additive Ions. *Chem. Mater.* **2019**, *31*, 7547–7557. [CrossRef]
34. Holz, M.; Heil, S.R.; Sacco, A. Temperature-dependent self-diffusion coefficients of water and six selected molecular liquids for calibration in accurate 1H NMR PFG measurements. *Phys. Chem. Chem. Phys.* **2000**, *2*, 4740–4742. [CrossRef]
35. Saharay, M.; Kirkpatrick, R.J. Water dynamics in hydrated amorphous materials a molecular dynamics study of the effects of dehydration in amorphous calcium carbonate. *Phys. Chem. Chem. Phys.* **2017**, *19*, 29594–29600. [CrossRef]
36. Alert, R.; Tierno, P.; Casademunt, J. Formation of metastable phases by spinodal decomposition. *Nat. Commun.* **2016**, *7*, 13067. [CrossRef]
37. Gebauer, D.; Gunawidjaja, P.N.; Bacsik, J.Y.P.; Ko, Z.; Aziz, B.; Liu, L.; Hu, Y.; Bergsröm, L.; Tai, C.W.; Sham, T.K.; et al. Proto-Calcite and Proto-Vaterite in Amorphous Calcium Carbonates. *Angew. Chem. Int. Ed.* **2010**, *49*, 8889–8891. [CrossRef]
38. Farhadi-Khouzani, M.; Chevrier, D.M.; Zhang, P.; Hedin, N.; Gebauer, D. Water as the Key to Proto-Aragonite Amorphous $CaCO_3$. *Angew. Chem. Int. Ed.* **2016**, *55*, 8117–8120. [CrossRef] [PubMed]
39. Kellermeier, M.; Raiteri, P.; Berg, J.K.; Kempter, A.; Gale, J.D.; Gebauer, D. Entropy drives calcium carbonate ion association. *ChemPhysChem* **2016**, *17*, 3535–3541. [CrossRef] [PubMed]
40. Saharay, M.; Yazaydin, A.O.; Kirkpatrick, R.J. Dehydration-Induced Amorphous Phases of Calcium Carbonate. *J. Phys. Chem. B* **2013**, *117*, 3328–3336. [CrossRef]
41. Bushuev, Y.G.; Finney, A.R.; Rodger, P.M. Stability and Structure of Hydrated Amorphous Calcium Carbonate. *Cryst. Growth Des.* **2015**, *15*, 5269–5279. [CrossRef]
42. Chao, Y.; Horner, O.; Vallée, P.; Meneau, F.; Alos-Ramos, O.; Hui, F.; Turmine, M.; Perrot, H.; Lédion, J. In Situ Probing Calcium Carbonate Formation by Combining Fast Controlled Precipitation Method and Small-Angle X-ray Scattering. *Langmuir* **2014**, *30*, 3303–3309. [CrossRef] [PubMed]